International Journal of Engineering Trends and Technology
ISSN: 2231 – 5381 / https://doi.org/10.14445/22315381/IJETT-V70I10P213
Volume 70 Issue 10, 111-123, October 2022

Original Article

Experimental Study and Analysis of Friction Stir Welding on Az-91Mg Alloy by using SEM

M. Yugandhar[1], B. Prabhakar Kammar[2], S. Nallusamy[3]

[1] *Department of Mechanical Engineering, Research scholar, Visvesvaraya Technological University-Jnana Sangama, Belgaum, Karnataka, India.*
(Research Center- New Horizon College of Engineering, Bengaluru), Bengaluru, India.
[2] *Department of Mechanical Engineering, Visvesvaraya Technological University-Jnana Sangama, Belgaum, Karnataka, India.*
(Gopalan College of Engineering and Management), Bengaluru, India.
[3] *Department of Adult, Continuing Education and Extension, Jadavpur University, Kolkata, India.*

[1]*Corresponding Author : yugandhar077@gmail.com*

Received: 26 July 2022 Revised: 12 September 2022 Accepted: 20 September 2022 Published: 19 October 2022

Abstract *- Due to the extremely reactive nature of Magnesium (Mg) alloys, fusion welding is complicated. In the presence of oxygen, magnesium quickly oxidized. As a result, solid-state fusion welding procedures are the ideal approaches for welding Mg alloys. In this research, AZ-91 Mg alloy sheets were bonded by Friction Stir Welding (FSW), and the joint quality was tested using microstructural investigations and microhardness measures. According to the findings, the joint was defect-free, and the size of the huge intermetallic that emerged in the base alloy was reduced. These findings point to Al dissolution in an Mg matrix. Micro hardness tests demonstrate the enhanced hardness in the weld zone caused by the FSW. The purpose of this article was to provide the findings of the butt joint quality of FSW samples of MgAlZn group alloys. Welding was done using the FSW tool at speeds ranging from 140 mm/min to 355mm/min. There is no porosity or cracking in the stir zone or its surroundings. As a result of the high grain refinement and enhanced precipitations at the grain boundaries, microhardness in the stir zone increased for all welds compared to the base metals. Metal plastic characteristics are likely to decline in certain locations. The findings indicate a substantial link between joint characteristics and welding conditions.*

Keywords *- Magnesium alloys, Friction stir welding, AZ9, Microstructure, Tensile examination, SEM.*

1. Introduction

The primary property of the material was strength to weight ratio of the weight of the particular material density of 1.735g/cm^3 and then compared to the base material of aluminum specific density of 2.34 g/cm^3. This material has a good damping property. Another characteristic of magnesium is its limited ductility and poor welding properties. The AZ-91 material is available on the market in the form of casting billets, which may be converted into slices and then back into the desired shape, such as rectangular, square, or round, and it has a very poor machining property as well as a very excellent damping property. AZ-91 material is mostly used nowadays for structures, the automobile, aerospace, medical, marine, and robotic industries, especially for end effectors for the Robot. We are triggering this material, especially when we decrease the weight [1, 2].

Among all the Aluminium-based magnesium combination AZ series material, especially in this material contains aluminum and zinc composition it has separate proportions are in terms different proportions, and this FSW process was explained by Mishra. Mating Magnesium alloy is very difficult by applying a normal welding process because this material easily reacts with oxygen, and easily the thermal property of this material is too high. Then we use the other fusion-based machining technique, friction stir welding. This process developed a solid-state phase fusion welding technique. It mated two comparable and non-similar junctions, and this challenges and constructing a metallurgical joint between AZ-91 and AZ-91 alloy by FSW process was completed. In this process, FSW carried out the tensile test and microstructure, Micro Vicker's hardness, and finally, the Scanning Electronic Microscope (SEM) test also eases use. Due to its relatively high strength, exceptional corrosion resistance, and superior cast ability, AZ-91 alloy is the most widely used kind of cast magnesium alloy. Plastic forming enhances the mechanical characteristics of die-casting AZ-91 alloy, and temperature is a key factor in this process. For the mechanical properties against plastic forming, it will be useful to understand how temperature affects yield stress and flow stress. The intermetallic compound of the $Mg_{17}Al_{12}$ phase, which predominately distributes along the grain boundary of the Mg phase, makes up a significant portion of the AZ-91 alloy. The phase strengthens the entire AZ-91 alloy at room temperature but weakens at high temperatures. Only a few

ten micrometers across the phase, and it is currently unknown how its characteristics will affect the complete family of AZ-91 alloys [3-5].

This work uses an indentation test to examine the mechanical properties of the microstructure in AZ-91D, and the characteristics of the $Mg_{17}Al_{12}$ and Mg matrix are assessed independently. Additionally, a FEM model of the AZ-91D alloy, which has both the $Mg_{17}Al_{12}$ and Mg phases, is constructed, and the experiment results are compared. After looking into the thermal degradation of both phases, the discussion will talk about how it affects the macroscopic deformation. Magnesium and its various alloys are suited for many industrial components due to its outstanding stiffness, low density, and electromagnetic protective characteristics. Magnesium alloy's practical uses are constrained by its severe disadvantages in terms of corrosion and hardness. Electro-less nano-coating is one of the newest techniques for enhancing magnesium alloy's corrosion resistance and hardness. This paper investigates the experimental investigation of corrosion and hardness of AZ-91 Mg alloy due to Nanocomposite techniques of ENi-B-TiO_2. The potential for improving the deposit efficiency and features of composite deposits by creating an appropriate bath composition and operation conditions should be thoroughly investigated, including experimental investigation [6, 7].

It has been shown that when Titania concentration increases, as the number of particles rises, so does the coatings' surface hardness. The ideal second phase (Titania) particle concentration and bath agitations are also investigated for better surface qualities after nano-coating. The materials may be used for a number of purposes in materials engineering after receiving this nano-coating [8-10].

2. Experimental Work

The compositions of magnesium alloy material are aluminium requires (8.1 to 9.30) but it contains 9.14%, zinc requires (0.4 to 1.0Max) but it contains 0.86%, manganese requires (0.13 to0.35 max) but it contains 0.2%, copper requires (0.10Max) but it contains 0.09%, silicon requires (0.2Max) but it contains 0.13%, ferrous requires 0.05% but it contains (0.01 percent), and nickel requires 0.01%. This AZ-91 particularly maintains a distinct composition alloy. This material was purchased from the exclusive magnesium alloy in Hyderabad, and the tool was H13 tool steel, and the form was a taper threaded pin with a length of 4mm, and with a width of 5mm, and a shoulder diameter of 15mm [11, 12].

The vertical CNC Milling machine was used to carry out the FSW procedure. The FSW procedure was carried out on a vertical CNC milling machine. 1200 rpm, 50 mm/min. The workpiece is carried on the bed of the vertical CNC milling machine shown in Figure 1(a), then inserting the tool by utilizing collect and chuck, and then finally gently applying the force and saddle moment between the workpiece and the work tool shown in Figures 1(b), (c) and (d) [13-16].

Fig. 1(a) Workpiece clamping

Fig. 1(b) Material sticking on the tooltip

Fig. 1(c) Material sticking on the tip with a Vowel shape

Fig. 1(d) CNC machining set up for FSW process

Then, using the axial force and rotational speed, begin the process of mating the two components. The tool will penetrate the workpiece up to the tool shoulder, and the shoulder will touch up to the workpiece surface at a depth of 4mm, and then the tool will travel with a 5mm breadth at the top and bottom and a 1mm length. The tool was rotated in the traverse direction. Then the process was started at 1200rpm and 50mm tool traverse speed, and the joint was obtained in a different condition from the workpiece start point and the endpoint. After doing the same practice, the process obtained the beads after mating the two pieces into a single butt joint. After successfully connecting the specimens [17-19].

Then, using a wire-cut Electric Discharge Machine (EDM), create a specimen measuring 28mm X 10mm X 6mm from the workpiece in a specific place. After the specimen was made, several types of graded emery sheets were used to polish it, followed by applying alumina paste and cleaning with ethanol. To begin chemical etching, several chemicals (5gm picric acid, 5ml acetic acid, 5ml distilled water, and 100ml ethanol) were used, and then the

specimen was washed with ethanol and dried using a drier machine. A polarised optical microscope was used for micro-structural observations [20-23].

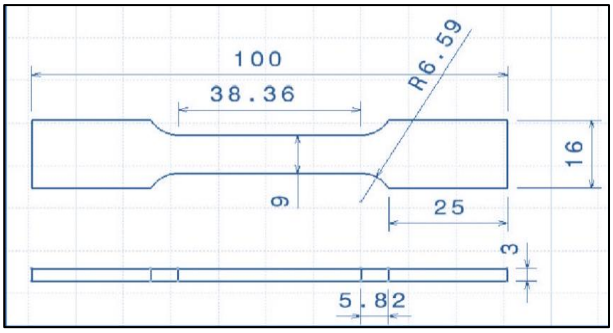

Fig. 2 Tensile test specimen specification

Micro Vickers hardness was performed utilizing a micro Vickers hardness machine and a total of ten indentions. The universal testing machine can reach the welding joint at a strong rate of (1.25X103 s1). Specimen preparation in accordance with ASTM Standard is shown in Figure 2 [9].

3. Result and Analysis

The above images depict the procedure, friction stir welding of Az-91 Mg alloys, and the joint created by utilizing a tool rotation speed of 1200 rpm and a tool traverse speed of 50 mm. As a result, the quantity of ($Mg_{17}Al_{12}$) phase AZ-91 Mg alloy in this same base material has the same brittleness and plastic deformation as AZ-91 Mg alloy. And previously, it was discussed how the base material reacts during the friction stir welding process, how the materials phase changes, and how thermal conductivity causes both the tool and the material to phase transform, causing the material to stick on the surface of the tool to stick, causing the material and the process to be interrupted or the process to stop.

This graphic demonstrates how the material behaves when it touches the tool and workpiece. This image depicts the difficulties of the machining process. It allows us to learn how the material deforms, fractures, and fails and how the material adheres to the tool. It indicates that if the plastic deformation is greater in this location, a failure may occur; the circles indicate how the mating of the parts may impact the failures. It results in the joint failing under the FSW process. In this research, cast AZ-91 magnesium alloy is subjected to quasi-static compression, tension, shear, and combined compression-shear tests to investigate its yield behavior. Shear-Compression Specimens (SCS), as opposed to complicated loading apparatus, are used to provide the extra shear stresses for the combined compression-shear tests.

Fig. 3(a) Material peeled while under stir process and also a hole through the top to the bottom

Fig. 3(b) Improper welding and material dragging

Results indicate that the SCS is useful for obtaining experimental findings under various stress levels. Due to its reliance on hydrostatic pressure and lode angle, the yield behaviors of AZ-91 Mg alloy cannot be well described. Three invariants of stress and deviatoric stress were included in the criteria. The second invariant of the deviatoric stress and the first invariant of the stress are quadratically associated. This standard can be used to characterize the AZ-91 Mg alloy experimental yield, as shown in Figures 3(a), (b), and (c).

Fig. 3(c) A contour hole made while under process

Thermal strains emerge when the dissipation of heat generated when welding AZ-91 / AZ-91 is not uniform owing to differences in thermal conductivity. This heat conductivity of the same alloy also demonstrates the attained flawless joint. It suggests a higher level of hot crack development during the welding of comparable metals. Thermal strains emerge when the dissipation of heat generated during welding AZ-91 and AZ-91 is non-uniform, owing to thermal conductivity differences. If these thermal stresses are not balanced, it results in hot fractures, as seen by a microscope in the current joint process at 1200 rpm and 50 mm/min feed. The total amount of heat generation in AZ-91alloy is different compared to AZ-91 alloy in this part at the same tool rotational speed. Traverse speed, and thus obtaining a set of parameters were avoiding the development of hot cracks, is an important job in joining AZ-91/AZ-91 alloys to get very strong metallurgical continuity [24, 25].

3.1. Mechanical Properties

According to the current FSW studies, FSW causes significant microstructural changes in the SZ coupled with TMAZ and HAZ. This modification has an effect on the mechanical qualities after welding. As a result, the mechanical characteristics of FSW of AZ-91 Mg alloy are examined and contained here.

3.1.1. Tensile Properties

The mechanical characteristics of AZ-91B mg alloy determined that inciting tool spin rate and decreasing welding rate increased joint tensile strength. Pareek et al. researched FSW for AZ-91B Mg alloy and discovered that the joint strength increases with the rotational rate. As per

the experiment, the processing parameters did not influence the tensile strength of FSW AZ-91B-H24. The effect of different tool materials on the FSW of AZ-91B Mg alloy was studied. It was discovered that the weld formed using HRC 66 high carbon tool steel and a shoulder diameter of 18mm. Pin profiles with threads demonstrated improved tensile characteristics [47].

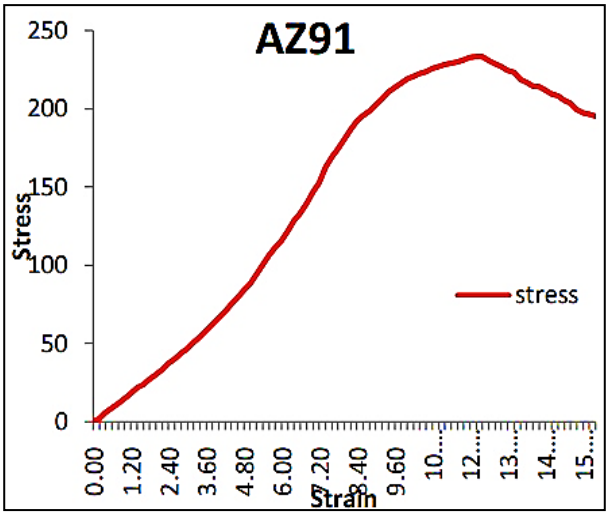

Fig. 4(a) Stress-strain curve of base metal tensile strength

Yield strength, elongation, and other transverse tensile characteristics of friction stir welded joint efficiency of AZ-91 magnesium alloy were investigated. Three specimens were tested, and the findings were averaged. First, the prepared specimens were examined and tested for tensile strength in universal testing equipment with a maximum tensile strength of five capacities in tonnes; tensile tension was applied at a rate of 2kN/min following ASTM recommendations. Displays the stress-strain curve of a base metal tensile specimen and the friction stir welded joint shown in Figure 4(a). The tensile strength of the base metal and FSW joint was 239.81MPa, and the yield strength of the base metal and the FSW joint were 199 MPa and 226.34 MPa, respectively189.625 MPa. Efficiency and lengthening of the joint observed were around 8% and 87%, respectively [27, 28].

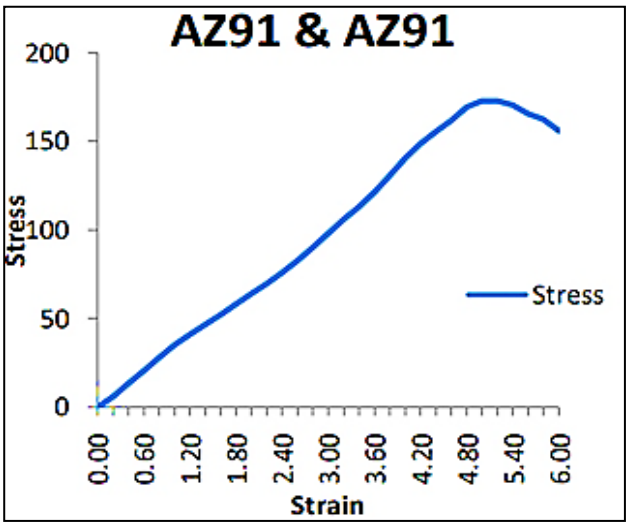

Fig. 4(b) Strain-stress curve of friction stir welded joint

The effect of tool pin diameter on the microstructure and material characteristics of FS spot welded AZ-91B mg alloy joints were investigated. Tensile shear force increased with increasing tool pin diameter for FS spot welded AZ-91B Mg alloy joints as the breadth and height of the curved interface influenced the specification failure as per experimental analysis investigates the AZ-91 mg alloy FS welded joint's microstructure and material properties. The findings show that the mechanical characteristics of the studied cross-section decrease from the higher to the lower direction of the joint, with the initial portion being the weakest and the center being the strongest.

To investigate the impact of the enhanced ten-fold cooling using air and water of the microstructure and substance FS welded AZ-91 mg alloy joint tensile characteristics, it disclosed that the ultimate tensile load with improved cooling conditions enhanced by 15.7%, and tensile deformation value increased by 10% 62.2%. According to excellent weld connections and higher. A pinless shoulder tool can be used to acquire mechanical characteristics. From AZ-91 Mg alloy FS welded investigated mechanical properties, FS welded AZ-91 mg alloy texture and microstructure response joints. Samples were tested with the FSW perpendicular direction as the primary axis showed greater strength levels than the basic material. The maximum tensile strength of the FSW parallel samples displayed elongation, as shown in Figure 4(b).

3.1.2 Micro Hardness

The hardness of different magnesium alloys varies with the amount of aluminum in them. Researchers also discovered that the hardness profile of any Mg alloy is impacted by grain size and precipitate dispersion in the weld. Microhardness was measured using a Vickers index test with a 100g load. The various zones impacted by hardness are depicted in Figure 5. The tool pin directly impacts material hardness [29-31].

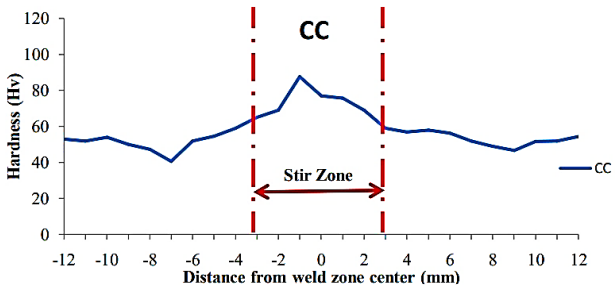

Fig. 5 Micro hardness measurement across FSW joint of similar metal AZ-91

The highest difference in hardness was achieved in the 3 to -3mm stir zone. The adjacent zone is the thermos mechanically impacted zone ranging from -3 to -5mm and 3 to 5mm. It exhibited a rising tendency comparable to the stir zone. The following zone is heat-impacted zones ranging from 5 to 10mm and -5 to -10mm, demonstrating a fall and rise in hardness towards the weld's center. The

following zone is base metal, which has shown a growing tendency when transitioning from HAZ to base material. The maximum hardness was discovered.

The effect of PWHT on the microstructures and mechanical characteristics of FSW welded AZ-91 mg alloy was investigated. The distribution of micro-Vickers hardness along the tool rotating axis near the weld interface demonstrates that the hardness near the weld interface is larger than that of the base metal. The work-hardened zone has the highest hardness value, which is found 3 to 6 mm away from the weld contact. The increased hardness is caused by grain refinement and works hardening Zone 87.67 for stirring Hv. Similarly, the hardness of the joint decreased from 87.67 to 40.67 Hv on the progressing side and from 87.67 to 40.67 Hv on the regressing side to 46.67 on the reversing side; similar findings were made with aluminum and magnesium alloys [32-38].

Since recrystallized fine grains in FSW contain some dislocations at the weld border, the higher hardness at the weld boundary is attributable to grain refinement. In contrast, the grain size in the work-hardened region is similar to that of the base material. As a result, the increased hardness here is attributed to work hardening. The hardness contour in the FSW joint is controlled by precipitate distribution and grain size, or both. The hardness value gradually decreased from around 73 HV through the TMAZ and HAZ to approximately 63 HV at the welds mid. The presence of the lowest hardness within the SZ is attributed to grain development and rapid recrystallization. Larger particle size when tool rotating speed increases. It leads to a decrease in hardness observed that increasing the rotational rate first raises the microhardness to a certain degree and then gradually decreases it. They identified two factors for the increase in hardness in the stir zone.

(i) Tiny intermetallic compound particles increase toughness.
(ii) The grain dimension of the stir zone is substantially smaller than that of the source material; grain modification plays a key role in metal strengthening here. An increased tool rotational rate creates more heat, which softens the material and results.

According to the researchers, the softening of the nugget zone/stir zone was caused by the dissolving of strengthening and coarsening of precipitates. The effect of tool pin diameter on the microstructure and material mechanical characteristics of an FS spot welded joint made of mg alloy AZ-91B was studied. They concluded that the smaller the pin, the microhardness of SZ, TMAZ, and HAZ. The effect of enhanced air and water cooling on the microstructure and material characteristics of the FSW welded AZ-91 mg alloy joint. They discovered that the microhardness of SZ rose significantly.

To investigate the work hardening performance, tensile strength, and microstructures of an FSW welded AZ-91B half-hardened H24 temper Mg alloy sheet at various temperatures. Several strain rates exist. They discovered that the hardness gradually decreased from approximately 70 HV in the base material to around 50 HV in the center of the joint. It is due to the formation of non-uniform cast structures in the friction zone and larger grain sizes in the FZ compared to the HAZ and BM. Studied the influence of process factors such as tool rotation rate and welding route using a cylindrical taper pin profile HSS tool at a fixed axial force on the characteristics of FSW welded AZ-91B Mg alloy lap joints. The effect of tool material and rotational rate on an FSW lap junction's microstructure and mechanical characteristics was investigated.

3.1.3. Impact Strength

The impact strength and joint efficiency of an AZ-91 magnesium alloy of friction stir the Charpy test analyzed welded joints. The average of three specimens was tested, and the results were concluded. Where catalysts for the development of onion rings and tiny grains. The mechanically impacted zone is next to the nugget zone. Deformed grain growth has been seen. It is grain size as a result of mechanical and thermal cycles [39- 41].

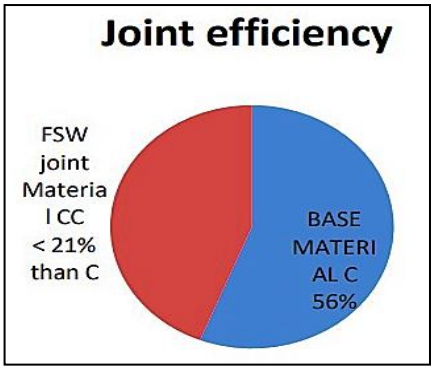

Fig. 6(a) Joint efficiency

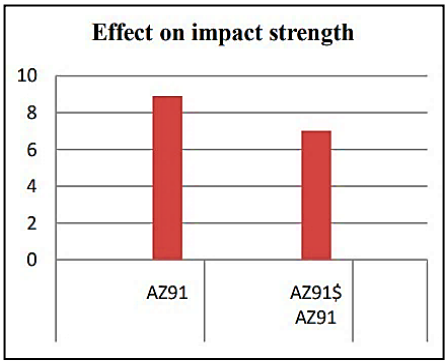

Fig. 6(b) Effect of impact strength on the base material and FSW joint of similar metal

The Charpy test sample has 50×16×6mm^3 dimensions, a 45^o V notch of 3mm depth, and a 0.35 mm root radius per ASTM guidelines. The impact strength of base metal and FSW joint was obtained at 9.35 J and 8.2 J, respectively, as shown in Figure 6(b). The efficiency of the joint was approximately 23% less than that of the base material, as shown in Figure 6(a) [42-44].

4. Micro Examination

The parent metal's microstructure, magnesium alloy, is on the right side of the FSW process. Primary alpha magnesium granules coexist with precipitated beta grains in the microstructure.

The beta grains are in the eutectic phase of $Mg_{17}Al_{12}$ zones. NZ and TMZ were created by heat as well as the HAZ. The nugget zone is roughly the same width as a pin with a diameter of around 6mm, where the FSW tool's shoulder has treated the sheet's surface. The microstructure reveals small fractured particles with alpha and beta grains shattered by frictional heat and stress.

The magnifications vary, but the field is the same, specifically the parent metal on the FSW process's left side. The parent metal appeared to be a magnesium alloy cast.

Fig. 7(a) Parent material 100X magnification

Fig. 7(b) Parent material 200X magnification

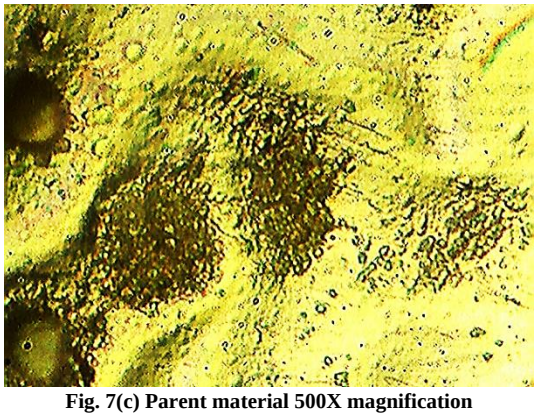

Fig. 7(c) Parent material 500X magnification

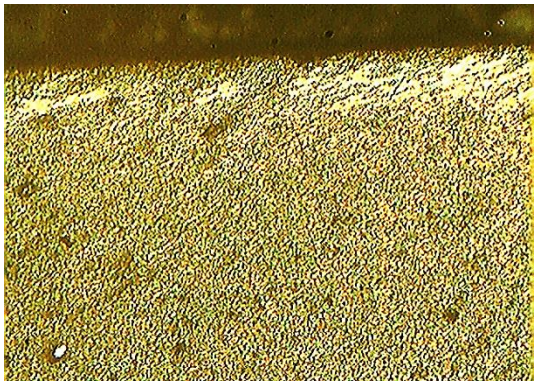

Fig. 7(d) Shoulder material 100X magnification

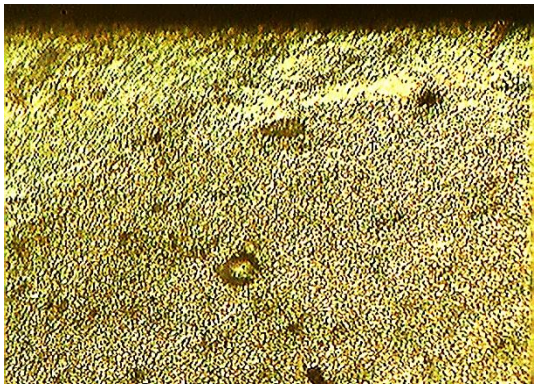

Fig. 7(e) Shoulder material 200X magnification

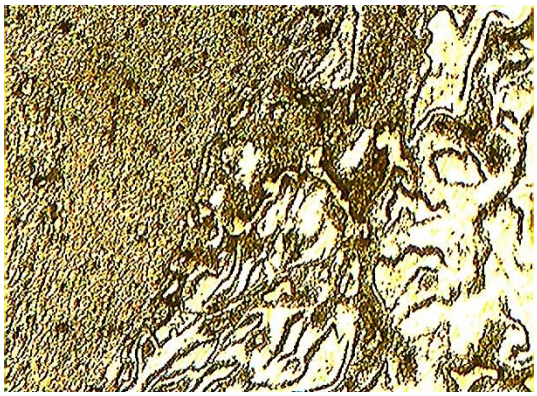

Fig. 7(f) Interface material 100X magnification

In the FSW process shoulder zone's microstructure, the FSW tool's shoulder has treated the sheet's surface. The microstructure reveals small fractured particles with both alpha and beta grains shattered by frictional heat and stress.

The optical microscope with low magnification was utilized to examine the square butt weld cross-section of the FSW collaboration Figure 7 depicts an optical microscopic cross-sectional view of an AZ-91 Mg friction stir weld junction at 1200 rpm rotation and 24mm/min welding speed. In the stir, there were three zones. The nugget zone is roughly the same width as a pin, with a diameter of around 6mm. Much research was examined on the stir zone onion ring-like structure seen in the midst of the weld. The creation of onion rings is caused by the ring-like motion of material in the stir zone. The instrument design of the tool shoulder, tool pin, and continuous deposition of molten base metal between the tool shoulder and pin.

These photomicrographs were taken at the FSW process's interface zone, which contains both the source metal Mg alloy and the treated nugget zone. The fusion line is the middle line. The heat-affected zone of the parent metal on the right side of the fusion line has experienced plastic deformation and has increased plasticity. The greater frictional heat produced the plasticity. Primary and secondary phase grains have both distorted. The NZ with minute broken grains is seen on the left side of the micrograph. Both alpha and beta grains are stretched along the tool's direction.

Fig. 7(g) Interface material 200X magnification

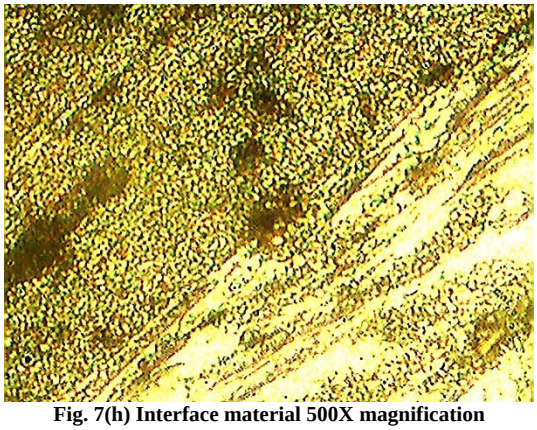

Fig. 7(h) Interface material 500X magnification

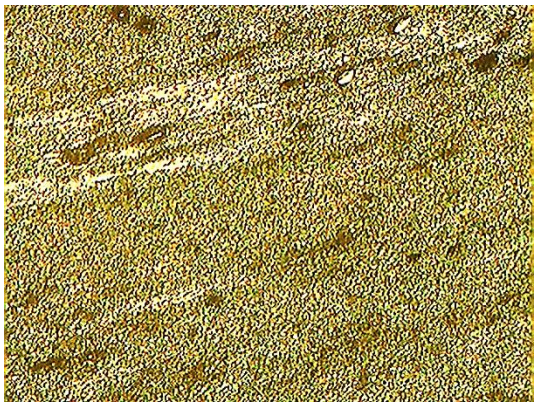

Fig. 7(i) Weld zone 100X magnification

These images were taken at the nugget zone's heart (refer to sketch). The alloy's microstructure displays small broken particles/grains in the bottom zone of the FSW process and the interface between the bottom parent metal and the nugget zone. The nugget zone is at the top of the picture, and the parent metal with elastically distorted grains is at the bottom.

The fusion line is the middle line. The heat-affected zone of the parent metal on the right side of the fusion line has experienced plastic deformation and has increased plasticity. The microstructure reveals small fractured particles with both alpha and beta grains shattered by frictional heat and stress.

Fig. 7(j) Weld zone 200X magnification

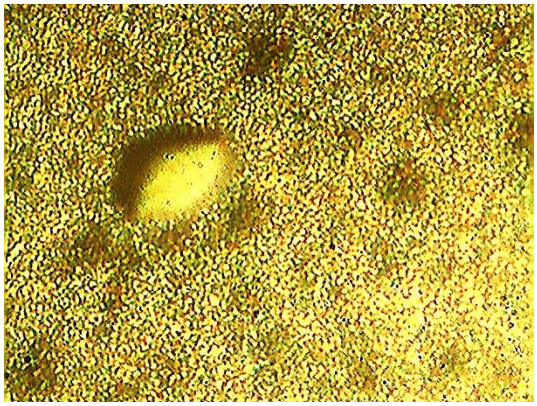

Fig. 7(k) Weld zone 500X magnification

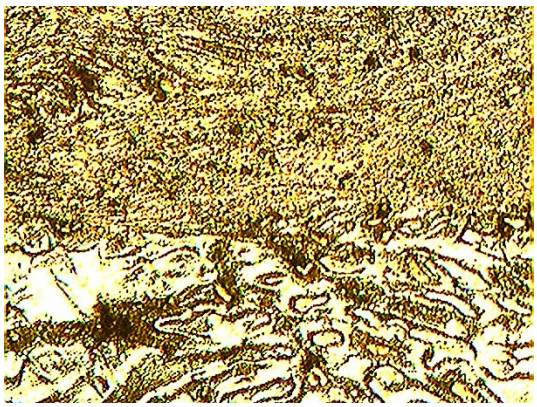

Fig. 7(l) Bottom weld zone 100X magnification

It contains both the source metal Mg alloy and the treated nugget zone. The fusion line is the middle line. The heat-affected zone of the parent metal on the right side of the fusion line has experienced plastic deformation and has increased plasticity. The microstructure reveals small fractured particles with both alpha and beta grains shattered by frictional heat and stress.

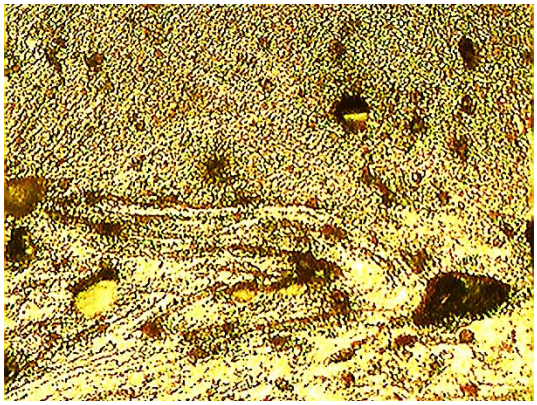

Fig. 7(m) Bottom weld zone 200X magnification

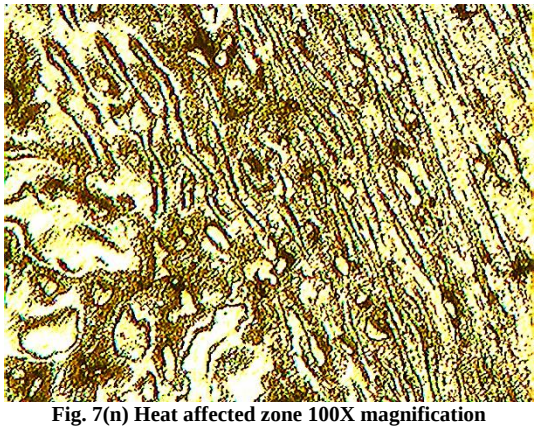

Fig. 7(n) Heat affected zone 100X magnification

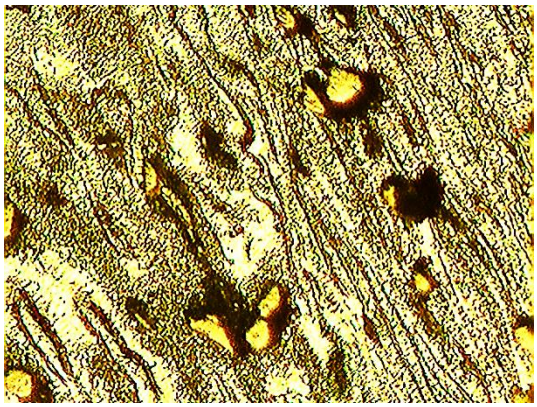

Fig. 7(o) Heat affected zone 200X magnification

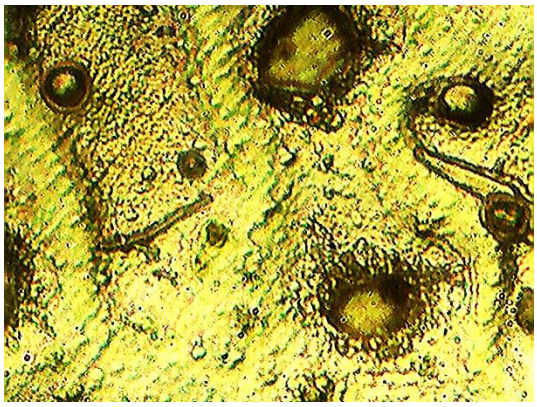

Fig. 7(p) Heat affected zone 500X magnification

The images show the parent metal heat-affected zone on the left side. The micrograph depicts the influence of heat and stress on grain movement and elongated grains at the nugget zone.

This image depicts the microstructure of the parent metal, Magnesium alloy, on the left side of the FSW process.

Fig. 7(q) Parent zone 100X magnification

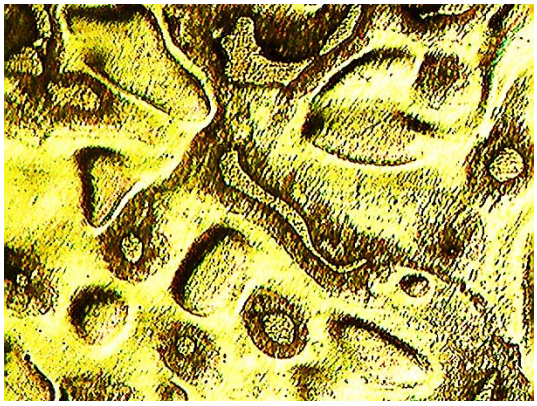

Fig. 7(r) Parent zone 200X magnification

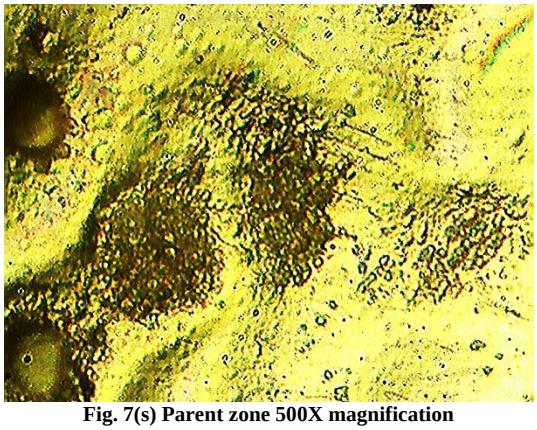

Fig. 7(s) Parent zone 500X magnification

Primary alpha magnesium granules coexist with precipitated beta grains in the microstructure. The beta grains are in the eutectic phase of $Mg_{17}Al_{12}$. Figures 7(a) to figure 7(s) are at various magnifications. The parent metal on the left side of the FSW process has the same name as the field.

5. Tensile Examination

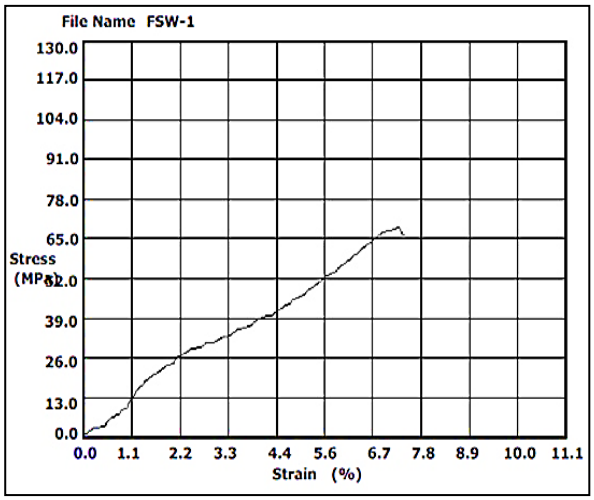

Fig. 8 Stress-strain relation, breaking point at 69.12<Mpa, and strain percentage at 7.1%

Figure 8 discusses the failure of the specimen in the center of the tool, i.e. where obtained the weld and find the length of elongation and stress/strain relationship under the weld. Tensile strength of 69.12mpa, yield strength of 60.12mpa, and elongation of 1.14% are the different numbers obtained from this graph. Following this test, the Micro Vickers hardness utilizing the prior micro examination samples. The parent metal on the left side of the FSW process has the same name as the field.

6. Tensile Fractography

Aluminum and steel may be replaced in many applications if the material can be made useful for high-temperature applications without raising the cost of the alloy, offering equivalent strength with less weight. Therefore, comparing various methods and alloys is necessary to obtain the ideal property needed in a specific situation. The material stress, strain, elongation, failures, and SEM analysis help us understand how the material behaves at the micron level. At a higher level, to employ this substance to assist the human body, and expect to see positive effects in the future. The different SEM images related to testing are shown in Figure 9(a) to Figure 9(i).

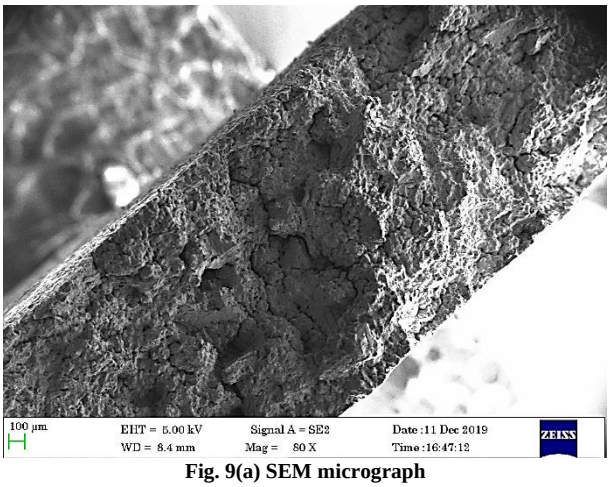

Fig. 9(a) SEM micrograph

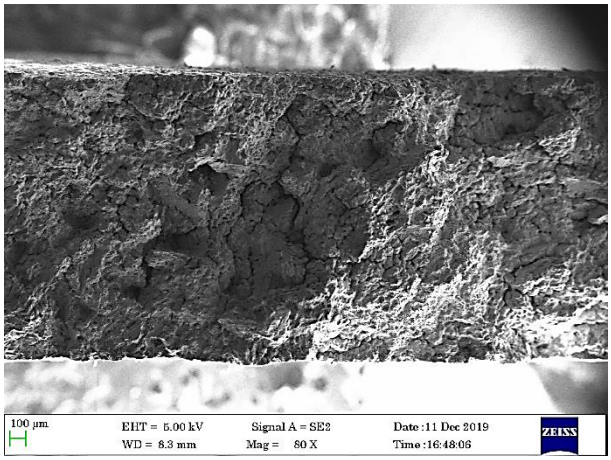

Fig. 9(b) SEM micrograph

SEM micrograph of the tensile test specimen's cracked surface. The fracture had formed in the heat-affected zone of the FSW joining procedure. The photo-macrograph depicts the shattered surface's tiny brittle surface morphology.

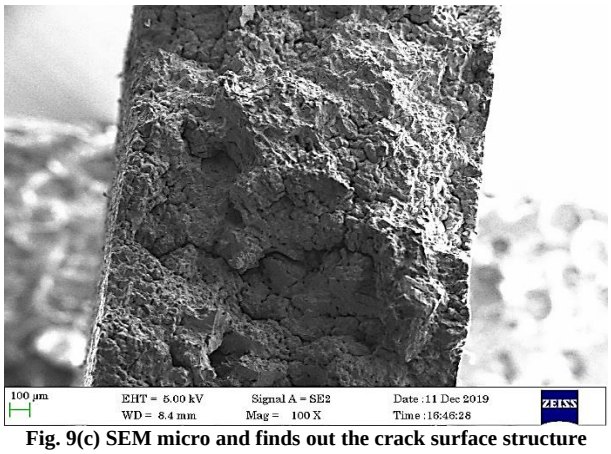

Fig. 9(c) SEM micro and finds out the crack surface structure

The macro graph also shows a huge dip, indicating a casting flaw. The two macrographs covered the whole fracture surface. The SEM has an 80X magnification. Figure 9(c) shows one field of the broken surface at 100X. The trough-like surface, which might be due to a casting flaw, has been rectified by the increased magnification. The magnesium alloy AZ-91 has favorable qualities that make it suitable for usage in the automotive and aerospace sectors. The alloy will be used more frequently, improving the car's fuel economy. The alloy's high-temperature uses are the main cause of worry. Aluminum and steel may be replaced in many applications. High-temperature applications can be useful without raising the cost of the alloy, offering equivalent strength with less weight. Therefore, comparing various methods and alloys is necessary to obtain the ideal property in a specific situation [46].

The enlarged picture of Figure 9(c) at 250X is seen in this SEM micrograph. The cracked surface has formed a thin crack perpendicular to the path of tension. In the heat-affected zone, the fracture appears as an intergranular crack running along the direction of grain movement.

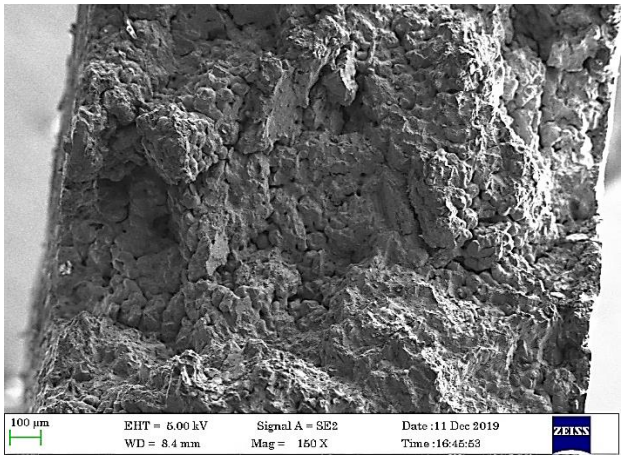

Fig. 9(d) SEM micro and finds out the crack surface structure and increased Magnification

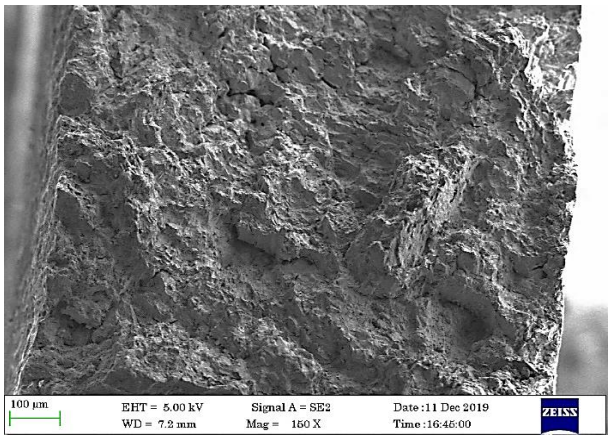

Fig. 9(e) SEM micro and finds out the crack surface structure and increased magnification and checks the crystalline structure

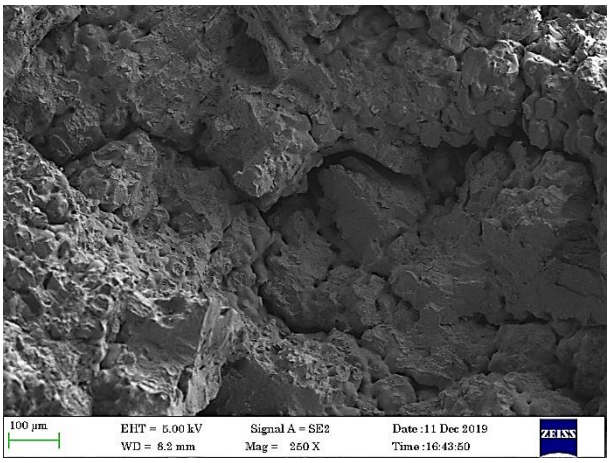

Fig. 9(f) SEM micro and finds out the crack surface structure and increased magnification and checks the crystalline structure and also at some place materials fail and shows crack surface

Figure 9(f) is a 250X SEM micrograph of the shattered surface. The broken surface morphology is brittle with a fine-grained fracture surface and no dimples.

Figure 9(g) depicts the fractured surface field with a huge trough, which might indicate a fault on the material's surface. The enormous trough at the fracture surface has been resolved by the increased magnification of 500X.

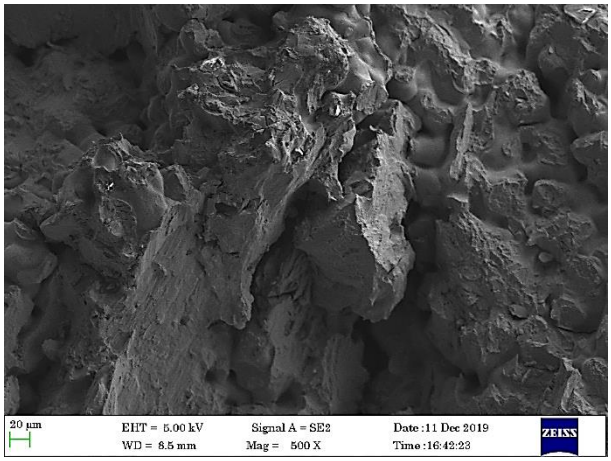

Fig. 9(g) Checks the crystalline structure and also, at some places, materials fail and show crack surface the crustal surface like in granular and valley surface formed intergranular surface running out and shuttered surface

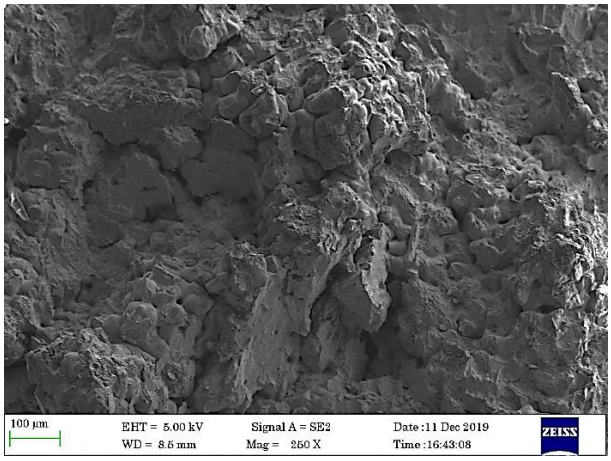

Fig. 9(h) checks the crystalline structure and also, at some place, materials fail, and shows ca rack surface the crustal surface like in granular, and valley surface formed intergranular surface running out

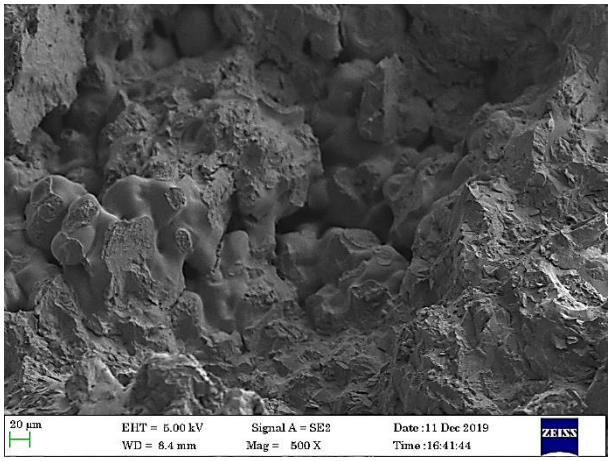

Fig. 9(i) depicts another fractured surface field with a deep trough that existed at the sample's shattered surface material

6.1. Fracture properties of FSW welded AZ-91 Mg alloys

Some investigations claim that in FSW of AZ-31Mg, UTS and tensile elongation are significantly reduced, owing to differences in texture, nugget form, and grain size. Some fracture performance studies revealed that

when the joint is loaded perpendicularly, the fracture may occur in the TMAZ or HAZ on the AS or RS of the weld joint, according to the FSW circumstances.

The variation in grain size is not the most important factor determining the fracture site of the FSW joint. To investigate the effect of textural alteration and twinning on AZ 91 Mg alloy fracture performance. They discovered various twinning actions. They found that the fracture locations at 1200 and 1600 rpm were the core of NZ and the TMAZ/NZ border. To investigate the microstructure and tensile fracture behavior of the FSW twin roll AZ-91 Mg alloy. They concluded that FSW right angle samples had the least strain to fracture, and fracture occurred between the SZ and the TMAZ in the AS. To investigate the fatigue fracture behavior of the FSW AZ-91 joint experimentally. They discovered that the fatigue specimens fractured along the HAZ at the AS at applied stress amplitudes.

7. Conclusion

Finally, based on the observed results, it was concluded that mating was successfully done by the two comparable Mg alloys AZ-91/AZ-91. This method is used in naval and aerospace equipment as well as structure frames. This FSW technique helps reduce total body weight compared to earlier aluminium alloys. It is one of the cheapest processes for combining two metals during the fusion welding stage.

The spinning tool speeds of 1200, 1400, and 1600 rpm, as well as the welding speeds of 12, 14, and 16 mm/s, created a loud friction stir. AZ-91 Magnesium alloy weld junction tensile characteristics were studied. This research finally discovered how the material stress, strain, elongation, failures, and SEM analysis help us understand how the material behaves at the micron level. At a higher level, that can employ this substance to assist the human body and expect to see positive effects in the future. The mechanical properties of the friction stir-welded joint of the magnesium alloy AZ-91 were improved by adding. Strengthened particles like Silicon aluminum oxide and carbide during the welding portion. Reinforced particles can be added. Yield strength at the weld portion was more expensive than basic metal. The results of Sic more strengthened particles on enhancing mechanical characteristics compared to aluminum oxide; however, its forms of reinforced particles improve mechanical characteristics in line with necessary applications and necessary mechanical attributes.

The tool pin diameter and profile, tool material, and shoulder diameter all substantially impacted joint characteristics. The primary source of heat created in FSW is friction between the workpiece and the tool shoulder. As a result, pin and shoulder sizes are more important than the FSW tool's design. Aside from the tool rotation rate and traverse velocity, the tilt angle of the tool relative to the specimen surface, axial force, and target height all play important roles in producing effective welds. In FSW, the welding temperature is governed by axial force. Material flow patterns are highly influenced by tool pin geometry, axial force flow stress of the material, and welding temperature. Aside from the butt and lap configurations, there are several study opportunities for T butt design of T lap junction, edge butt joint, multiple lap weld joint, and fillet weld joint for various applications. The basic material microstructure is transformed during the FSW process, resulting in the creation of SZ, TMAZ and HAZ. Each zone's microstructure, grain size, precipitate size and distribution, and dislocation density are unique.

Because of the considerable deformation, significant residual stresses are created during the FSW process. Tensile residual stresses exist in TMAZ and SZ, whereas residual compressive stresses exist in HAZ. The weld advancing edge has a higher residual stress intensity than the receding edge. The FSW factors and conditions have a significant impact on the mechanical characteristics of the material after weld. The increased hardness in the stir area/nugget is caused.

- The breadth of the friction stir zone was 4 .5mm to 2.8 mm taper, which was identical to the diameter of the pin.
- Non-uniform and irregular grains were discovered in base metal, transition zone, and heat treatment. During friction stir welding, an impacted zone and homogenous grains were detected in the stir zone.
- Because of dynamic recrystallization, the stir zone featured fine grain and equiaxed grains. Heat impacted zone and Thermo mechanically affected zone.
- The tensile strength of the base metal and the FSW joint were 238.61MPa and 196.4MPa, respectively. The yield strength of the base metal and the FSW joint were 199.98MPa and 185.76MPa, elongation of roughly 8.2%, and joint efficiency of nearly 87%.

Future work

1. Individual researchers use a variety of tools, according to previously published literature. However, a tool with a cylindrical pin and a concave-shaped shoulder is seldom used for FSW of AZ-91 Mg alloy. Specific profile pin tools have also been developed, and there is a large research scope for developing and implementing unique profile tools, although this requires explanation.
2. To manufacture defect-free and sound weld joints, selection criteria for FSW method variables (rotational tool rate, tool traverse velocity, axial force, and tool tilt) are critical and must be standardized.
3. Apart from butt and lap joint arrangement, investigators must explore additional joint specifications for the real-time deployment of FSW in the industry.
4. More research is needed to understand the impact of FSW variables and alloy composition on the microstructure and grain size of FSW weld AZ-91 Mg alloys.
5. Material flow during FSW is quite complex. Phenomena that still require additional investigation.

6. To reduce the produced residual stresses during AZ-91 magnesium alloy FSW, proper FSW parameters must be used. Heat treatment following FSW can improve the mechanical qualities of the joint. As a result, future studies can focus on this area as well.

Reference

[1] S. Nallusamy et al., "Analysis of Welding Properties in FSW Aluminium 6351 Alloy Plates Added with Silicon Carbide Particles," *International Journal of Engineering Research in Africa*, vol. 21, pp. 110-117, 2016.

[2] B. L. Mordike and T. Ebert, "Structural Materials: Properties, Microstructure and Processing," *Materials Science and Engineering: A*, vol. 302, pp. 37-45, 2001.

[3] H. E. Fridrich and B. L. Mordike, "Magnesium Technology," *Springer*, Germany, 2006.

[4] F. Czerwinski and F. Czerwinski, "Welding and Joining of Magnesium Alloys, Magnesium Alloys – Design," *Processing and Properties*, Croatia, 2011.

[5] R.S. Mishra, Z.Y. Ma, "Friction Stir Welding and Processing," *Materials Science and Engineering: R: Reports*, vol. 50, no. 1-2, pp. 1-78, 2005.

[6] R. S. Mishra, P. S. De and N. Kumar, "Friction Stir Welding and Processing," *Science and Engineering*, 2014. Doi: 10.1007/978-3-319-07043-8_2.

[7] A. C. Somasekharan, L. E. Murr, "Microstructures in Friction-Stir Welded Dissimilar Magnesium Alloys and Magnesium Alloys to 6061-T6 Aluminum Alloy," *Materials Characterization*, vol. 52, no. 1, pp. 49-64, 2004.

[8] C.Y. Lee, W.B. Lee, Y.M. Yeon and S.B. Jung, "Friction Stir Welding of Dissimilar Formed Mg Alloys (AZ31/AZ-91)," *Materials Science Forum*, vol. 486-487, pp. 249-252, 2005.

[9] "ASTM Standard, E8/E8M-11, Standard Test Methods for Tension Testing of Metallic Materials," *ASTM International*, West Conshohocken, PA, USA, 2009. Doi: 10.1520/E0008_E0008M-11.

[10] R. W. Messler, "Principles of Welding: Processes, Physics, Chemistry and Metallurgy," *Wiley India Pvt. Ltd*, New Delhi, 2004.

[11] R. S. Parmar, "Welding Engineering and Technology," *Khanna Publishers*, New Delhi, 2010.

[12] B. Ratna Sunil, G. Pradeep Kumar Reddy, A. S. N. Mounika, P. Navya Sree, P. Rama Pinneswari, I. Ambica, R. Ajay Babu and P. Amarnadh, "Joining of AZ31 and AZ-91 Mg Alloys by Friction Stir Welding," *Journal of Magnesium and Alloys*, vol. 3, pp. 330-334, 2015.

[13] Prakash Kumar Sahu and Sukhomay Pal, "Multi Response Optimization of Process Parameters in Friction Stir Welded AM20 Mg Alloy by Taguchi Grey Relational Analysis," *Journal of Magnesium and Alloys*, vol. 3, pp. 36-46, 2015.

[14] V. Jaiganseh and P. Sevvel, "Effect of Process Parameters on Microstructural Characteristics and Mechanical Properties of AZ80A Mg Alloy During Friction Stir Welding," *The Indian Institute of Metals*, vol. 68, pp. S99-S104, 2015.

[15] Bhukya Srinivasa Naik et al., "Residual Stresses and Tensile Properties of Friction Stir Welded AZ31B-H24 Mg Alloy in Lap Configuration," *Metallurgical and Materials Transactions B*, vol. 46, pp. 1626-1637, 2015.

[16] S. Mironov et al., "Microstructure Evolution during Friction Stir Welding of AZ31 Mg Alloy," *Acta Materialia*, vol. 9, pp. 301-312, 2015.

[17] P. Sevvel and V. Jaiganesh, "Characterization of Mechanical Properties and Microstructural Analysis of Friction Stir Welded AZ31B Mg Alloy through Optimized Process Parameters," *Procedia Engineering*, vol. 97, pp. 741-751, 2014.

[18] B. S. Naik, and D. L. Chen, "Texture Development in a Friction Stir Lap Welded AZ1B Mg Alloy," *The Minerals, Metals and Materials Society*, vol. 45, no. 10, pp. 4333-4349, 2014.

[19] Yong zhao et al., "Microstructure and Mechanical Properties of Friction Stir Welded MG2Nd- 0.3Zn-0.4Zr Mg Alloy," *Journal of Materials Engineering and Performance*, vol. 23, pp. 4136-4142, 2014.

[20] S. Ugender and A. Kumar, "Microstructure and Mechanical Properties of AZ31B Mg Alloy by Friction Stir Welding," *Procedia Material Science*, vol. 6, pp. 1600-1609, 2014.

[21] Inderjeet Singh and Gurmeet Singh Cheema, "An Experimental Approach to Study the Effect of Welding Parameters on Similar Friction Stir Welded Joints of AZ31B-O Mg," *Advances in Materials Science and Engineering: An International Journal*, vol. 2, no. 4, pp. 837-846, 2014.

[22] S. Rajakumar and A. Razalrose, "Friction Stir Welding of AZ61A Mg Alloy," *Advanced Manufacturing Technology*, vol. 68, pp. 277-292, 2013.

[23] S. H. Chowdhury et al., "Friction Stir Welded AZ31 Mg alloy, Microstructure, Texture and Tensile Properties," *The Minerals, Metals and Materials Society*, vol. 44, pp. 323-336, 2012.

[24] A. Razal Rose and K. Manisekar, "Influences of Welding Speed on Tensile Properties of Friction Stir Welded AZ61A Mg alloy," *Journal of Materials Engineering and Performance*, vol. 21, pp. 257-265, 2011.

[25] K. L. Harikrishna et al., "Friction Stir Welding of Mg Alloy ZM21," *Transactions of the Indian Institute of Metals*, vol. 63, pp. 807-811, 2010.

[26] Raju Kamminana, Venkatasubbaiah Kambagowni, "Modeling and Optimization of Process Parameters of Friction Stir Welding of Al-Li Alloy AA2050 by Response Surface Methodology," *SSRG International Journal of Engineering Trends and Technology*, vol. 69, no. 5, pp. 208-227, 2021. *Crossref*, https://doi.org/10.14445/22315381/IJETT-V69I5P228

[27] R. S. Pishevar et al., "Influences of Friction Stir Welding Parameters on Microstructural and Mechanical Properties of AA5456 (Almg5) at Different Lap Joint Thicknesses," *Journal of Materials Engineering and Performance*, vol. 24, pp. 3835-3844, 2015.
[28] Nallusamy, S., Karthikeyan, A., "Synthesis and Wear Characterization of Reinforced Glass Fiber Polymer Composites with Epoxy Resin Using Granite Powder," *Journal of Nano Research*, vol. 49, no. 1, pp. 1-9, 2017.
[29] A. Kouadrihenni et al., "Mechanical Properties, Microstructure and Crystallographic Texture of Magnesium AZ-91-D Alloy Welded by Friction Stir Welding," *Metallurgical and Materials Transactions*, vol. 45A, pp. 85-92, 2014.
[30] P. Sevvel et al., "Characterization of Mechanical Properties and Microstructural Analysis of Friction Stir Welded AZ31B Mg Alloy through Optimized Process Parameters," *Procedia Engineering*, vol. 97, no. 741-751, 2014.
[31] J. Yang and D. R. Ni, "Strain Controlled Low Cycle Fatigue Behavior of Friction Stir Welded AZ31 Magnesium Alloy," *Metallurgical and Materials Transactions*, vol. 45A, pp. 90-99, 2013.
[32] J. Yang et al., "Effects of Rotation Rates on Microstructure, Mechanical Properties and Fracture Behavior of Friction Stir Welded AZ31 Magnesium Alloy," *Metallurgical and Materials Transactions*, vol. 44A, pp. 101-109, 2012.
[33] Lechoslaw Tuz et al., "Friction Stir Welding of AZ-91 and AM Lite Magnesium Alloys," *Welding International*, vol. 27, no. 4, pp. 265-267, 2013.
[34] Nallusamy, S., "A Review on the Effects of Casting Quality, Microstructure and Mechanical Properties of Cast Al-Si-0.3Mg Alloy," *International Journal of Performability Engineering*, vol. 12, no. 2, pp. 143-154, 2016.
[35] Kazuhiro Nakata, "Friction Stir Welding of Magnesium Alloys," *Welding International*, vol. 23, no. 5, pp. 328-332, 2009.
[36] B. Ratna Sunil et al., "Joining of AZ31 and AZ-91 Mg Alloys by Friction Stir Welding," *Journal of Magnesium and Alloys*, vol. 3, no. 4, pp. 330-334, 2015.
[37] Juan chen et al., "Double Sided Friction Stir Welding of Magnesium Alloy with Concave Convex Tools for Texture Control," *Materials and Design*, vol. 76, pp. 1-10, 2015.
[38] H. M. Rao et al., "Friction Stir Spot Welding of Rare Earth Containing ZEK 100 Magnesium Alloy," *Materials and Design*, vol. 56, pp. 1-14, 2015.
[39] A. Dorbane et al., "Mechanical Microstructural and Fracture Properties of Dissimilar Welds Produced by Friction Stir Welding of AZ31B and Al6061," *Material Science and Engineering*, vol. 5, pp. 62-70, 2015.
[40] R. Z. Xu et al., "Pinless Friction Stir Spot Welding of Mg-3Al-1Zn Alloy with Interlayer," *Journal of Material Science and Technology*, vol. 18, pp. 52-62, 2015.
[41] Nallusamy, S., "Thermal Conductivity Analysis and Characterization of Copper Oxide Nanofluids through Different Techniques," *Journal of Nano Research*, vol. 40, pp. 102-112, 2015.
[42] S. Malopheyev et al., "Friction Stir Welding of Ultra Fine Grained Sheets of Al-Mg-Sc-Zr Alloy," *Materials Science and Engineering*, vol. 624, pp. 132-139, 2015.
[43] H. M. Rao et al., "Effect of Process Parameters on Microstructure and Mechanical Behaviors of Friction Stir Linear Welded Aluminium to Magnesium," *Material Science and Engineering*, vol. 651, pp. 27-36, 2015.
[44] Banglong Fu et. al., "Friction Stir Welding Process of Dissimilar Metals of 6061-T6 Aluminum Alloy to AZ31B Mg Alloy," *Journal of Material Processing Technology*, vol. 218, pp. 38-47, 2015.
[45] Santhosh V, Natarajan U, "Evaluation of Temperature Distribution of Solid State Welded AA6061Alloy," *SSRG International Journal of Mechanical Engineering*, vol. 6, no. 2, pp. 13-16, 2019. Crossref, https://doi.org/10.14445/23488360/IJME-V6I2P103
[46] M. M. Avedesian and H. Baker, "ASM Specialty Handbook, Magnesium and Magnesium Alloys," *ASM International*, USA, 1999.
[47] G. Padmanabhan and V. Balasubramanian, "An Experimental Investigation on Friction Stir Welding of AZ31B Mg Alloy," *Journal of Advanced Manufacturing Technology*, vol. 49, pp. 111-121, 2009.